analytical chemistry

pubs.acs.org/ac Letter

# Ratio-Adjustable Upconversion Luminescence Nanoprobe for Ultrasensitive In Vitro Diagnostics

Jianxiong Zhou,[‖] Ruiying Wu,[‖] Xiao Fu, Jinmei Wu, and Qingsong Mei*

Cite This: https://doi.org/10.1021/acs.analchem.1c01537 Read Online

ACCESS | Metrics & More | Article Recommendations | Supporting Information

**ABSTRACT:** The development of precise medicine requires diagnostic probes to simultaneously satisfy an excellent detection limit and a wide linear analysis range because of enormous individual-discrepancy of disease biomarker concentrations, yet it remains challenging. Herein, an upconverison nanoprobe with a luminescence ratio flexibly tailored was designed for ultrasensitive monitoring exhaled nitric oxide to indicate the clinical course of asthma. Two independent emissions from the same nanoprobe can be discretionarily modulated to vary their intensity ratios for adapting different analysis requirements. Delightfully, this novel nanoprobe demonstrated a 100-fold lower detection limit compared with the traditional ratiometric fluorescence manner and a more broad linear detection range from the subpart per billion (ppb) level to hundreds of ppb. This ratio-adjustable fluorescence detection strategy holds great potential for miscellaneous disease diagnosis applications.

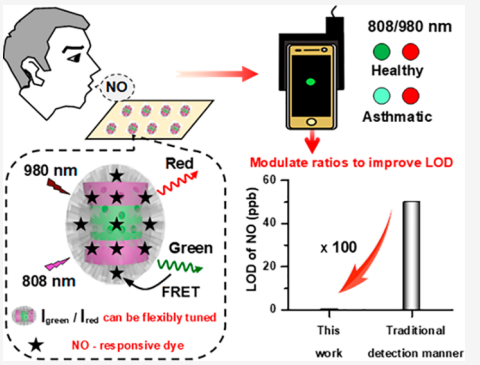


Downloaded via UNIV OF LIVERPOOL on July 11, 2021 at 18:30:24 (UTC).
See https://pubs.acs.org/sharingguidelines for options on how to legitimately share published articles.

Precise and rapid medical diagnosis of biomarkers plays a pivotal role in disease-prevention, therapy, and prognosis. Volatile organic compounds (VOCs) in exhaled gas have been recognized as important biomarkers for many diseases, such as cancer, diabetes, and so on.[1,2] As typical breath VOCs, exhaled nitric oxide (NO) has been deemed as a prognostic biomarker for a few chronic respiratory ailments, such as emphysema, bronchitis, and asthma.[3,4] It has been evidenced that NO levels in breath gas will increase due to the activation of inducible NO synthase in airway epithelial cells.[5] The relative concentrations of NO are changed in the pathologic course of asthma and markedly different during physiological processes associated with an individual's age, sex, and smoking habits, which may vary from a subppb level of healthy adults to hundreds of ppb level of asthma adults,[6] making its precise analysis a challenging assignment. Despite many sensing strategies, such as gas chromatography−mass spectrometry and microchip-based methods, that have been applied to monitor NO,[7−11] these methods are suffering from disadvantages of being time-consuming and requiring professional training, which is not suitable for in-field and ultrasensitive analysis applications. Therefore, it is indispensable to explore portable detection strategies to improve the instant sensing-performance for breath analysis.

Fluorescent sensors provide multiple information on complex systems, such as target concentrations and distributions, in the terms of intensity quenching or recovery, thus they are widely explored in biomedical imaging and clinical diagnostics.[12−14] With respect to the detection accuracy, usage of single emission is always problematic attributed to a few target-independent external interferences of the microenvironment around the probes, for instance, photobleaching or fluctuation of excitation light.[15,16] Multiple emission-based ratiometric fluorescence probes, possessing a self-calibrating signal from different but correlated emissive centers, have been demonstrated to powerfully minimize the external influence.[17−19] Moreover, ratiometric fluorescent sensors exhibit more distinctive color changes that are beneficial for naked eye-based on-site detection.[20,21] Nowadays, the reported ratiometric fluorescence probes usually explore dual emission signals, in which one plays the interior reference that is target-irresponsive, to calibrate the detection signal that the other emission acts as.[22,23] However, these dual emission signals always are highly dependent, i.e., the reference signal simultaneously increases or decreases along with the detection signal. To improve the detection sensitivity, the detection signal sometimes needs to modulate the weaker signals to lower the limit of detection. In this case, the reference signal also will be very weak, which is not able to accurately calibrate the microenvironmental interferences. Moreover, the weak detection signal is not suitable for high-concentration target analysis because the fluorescence response is easy to be saturated. One key to simultaneously achieve a sensitive and broad linear correlation range for quantitative analysis of exhaled VOCs lies in the development of novel ratiometric detection techniques.

**Received:** April 11, 2021
**Accepted:** June 28, 2021


© XXXX American Chemical Society

https://doi.org/10.1021/acs.analchem.1c01537
Anal. Chem. XXXX, XXX, XXX−XXX

Herein, we experimentally demonstrated a novel ratiometric fluorescence analysis strategy based on orthogonal emissive upconversion nanoparticles (UCNPs), where dual emission intensities at different excitation conditions can be independently modulated. To achieve sensitive detection of breath volatile NO gas, recognition unit rhodamine derivatives (Rd) were encapsulated into a mesoporous silica layer on the surface of the UCNPs. In this nanoprobe, green colored emission at 808 nm excitation acted as a detection signal, and its intensity can be modulated to be quite weak for lowering the detection limit. Meanwhile, the intensity of the red emission at 980 nm excitation can be tailored to be bright according to the requirements. The combination of NO molecules in exhaled gas with Rd distinctively quenched green emissions while unaffecting red emission intensities. This characteristic color changes on test paper were feasibly monitored by a smartphone-based analysis platform (Figure 1). Comparing

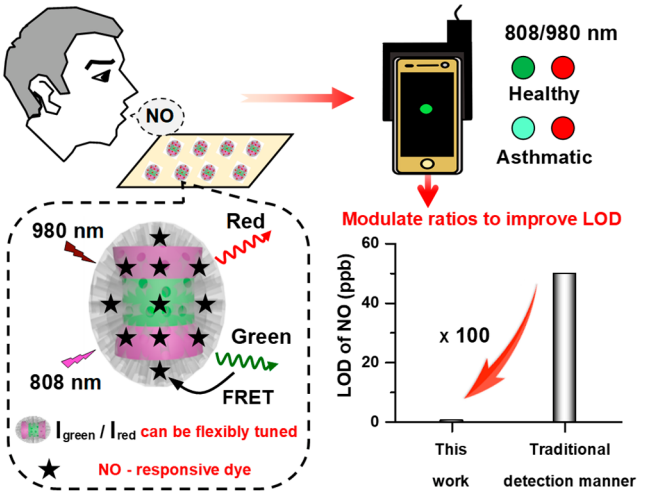


**Figure 1.** Schematic illustration of the composition of the ratio-tunable upconversion nanoprobe and the working principle for detection of NO in exhaled breath. The intensity ratios of green to red emission of the nanoprobe can be discretionarily modulated by changing the 980 and 808 nm excitation powers. The detection limit (LOD) of this ratio-tunable nanoprobe is greatly improved by 100-fold compared with the traditional detection manner in which the intensity ratio is fixed.

with a normal ratiometric fluorescent probe, the intensity ratios of green emission to red emission can be flexibly modulated, making the probe demonstrate a 100-fold lower detection limit and possess a large linear detection range from the subppb level to hundreds of ppb.

## RESULTS AND DISCUSSION

To achieve the flexible ratio-modulation, dual emissions of the same system should be independently varied through external stimuli. Lanthanide ions possess abundant ladderlike energy levels, facilitating the realization of such independent multiple-emissions.[24−26] In this work, the energy migration process of lanthanide activator ions was designed to be manipulated through locating different sensitizer ions in diverse particle layers. As we previously reported, the orthogonal emissive UCNPs, $NaErF_4$:Yb/Tm@$NaYF_4$:Yb@$NaNdF_4$:Yb, were synthesized by a layer-by-layer coprecipitation approach.[27−29] The transmission electron microscopy (TEM) image in Figure 2a

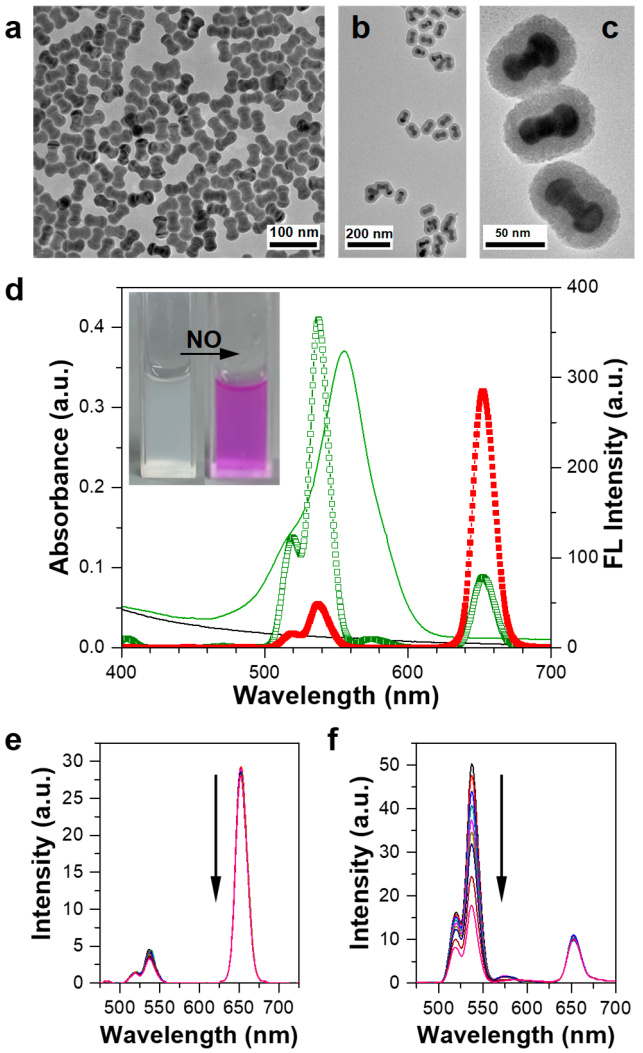


**Figure 2.** Characterization of the nanoprobe and detection of NO in aqueous solution. TEM images of the orthogonal emissive UCNPs (a) and mesoporous silica coated UCNPs (b,c). (d) Absorption spectra (solid lines) of the recognition molecules Rd before (black) and after (green) reaction with NO. Luminescent spectra (dotted lines) of the mUCNPs upon excitation with 980 nm (red) and 808 nm (green) excitation. The inset image shows color changes of the dyes Rd before and after reaction with NO. (e,f) Luminescent variations of the nanoprobe after additions of different amounts of NO upon excitation with 980 nm (e) and 808 nm (f). The concentrations of NO in parts e and f from the top to bottom are 0, 10, 20, 30, 40, 50, 60, 80, and 100 $\mu$M, respectively.

demonstrates that the dumbbell shaped UCNPs exhibited a uniform size with a width of approximately 22 nm and length of about 50 nm (Figure S1). X-ray diffraction patterns showed that the obtained UCNPs were indexed to the hexagonal phase nanocrystals (Figure S2). To improve the particles' water-dispersibility and provide an anchoring site for Rd molecules, the mesoporous silica layer with a thickness of 20 nm was successfully coated onto the surface of the UCNPs (Figure 2b,c). The appearance of a stretching vibration peak of a hydroxyl group and a Si−O bond in the Fourier transform-infrared spectra also verified this point. Moreover, the adsorption of Rd molecules in mesoporous silica can be validated through a zeta potential variation (Figure S2), and a saturated adsorbed amount of Rd molecules in the mesoporous


https://doi.org/10.1021/acs.analchem.1c01537
Anal. Chem. XXXX, XXX, XXX−XXX

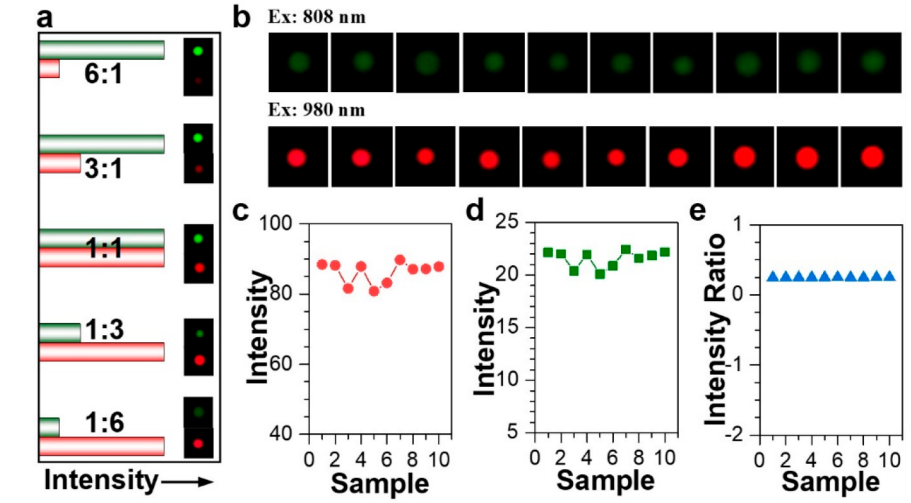


**Figure 3.** Tunable intensity ratio and the stability investigations of red and green emissions on the test paper. (a) Different intensity ratios upon modulation of 980 and 808 nm laser powers. (b) Luminescent image of 10 different blank test paper upon 808 and 980 nm excitation. (c–e) Intensity of red emission (c) and green emission (d) and intensity ratio of green to red emission (e) on the test paper.

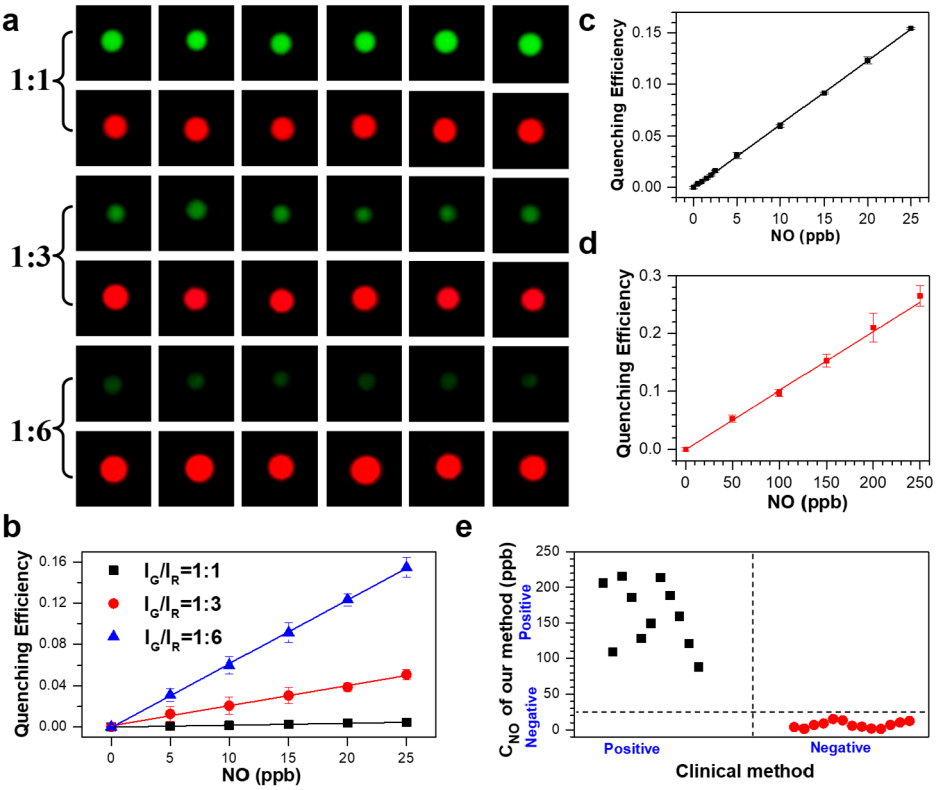


**Figure 4.** Detection of NO exhaled gas: (a) detection of exhaled NO gas by the use of the test paper upon modulation of the intensity ratio to be 1:1, 1:3, and 1:6 by adjusting the laser power. The amounts of NO from left to right are 0, 5, 10, 15, 20, and 25 ppb for each panel, respectively. (b) The corresponding quenching efficiency of the test paper at different intensity ratios. (c) Linear response of quenching efficiency with intensity ratios of 1:6 toward exhaled NO in the range of 0.5–25 ppb. (d) Linear response of quenching efficiency with intensity ratios of 1:3 toward exhaled NO in the range of 50–250 ppb. (e) Asthma diagnostics by use of our method compared with the clinical method.

silica was calculated to be 4.4 mmol Rd per 1 mmol mUCNPs according to the linear plot in Figure S3b.

As we expected, the mesoporous silica coated UCNPs (mUCNPs) gave out red light upon excitation at 980 nm and emitted green light under excitation with 808 nm light (Figure 2d). The recognition molecules Rd were colorless and exhibited a negligible absorption in the visible spectrum region. After exposure to NO gas, Rd molecules became purple and demonstrated a broad absorption peak in the green light region but still no absorption in the red light region. The reaction mechanism was demonstrated in Figures S5 and S6. Thus, the red emission of mUCNPs was retained unchanged upon exposure to different amounts of NO; however, green emission at 808 nm excitation showed a gradual quenching


https://doi.org/10.1021/acs.analchem.1c01537
Anal. Chem. XXXX, XXX, XXX−XXX

behavior due to the resonance energy transfer mechanism (Figure 2e,f). In detail, green emission at 808 nm excitation exhibited a gradual quenching with increasing NO concentrations, and the quenching efficiency reached 64.57% when the NO concentration raised to 100 $\mu$M. However, red emission at 980 nm excitation showed ignorable quenching when increasing the NO amounts (Figure S7). The nanoprobe also demonstrated an excellent selectivity toward many interfering anion ions because of the highly specific reaction between NO and Rd molecules (Figure S8).

Rapid and portable detection of exhaled NO requires development of simple analysis devices. In this work, the Rd modified mUCNPs-based nanoprobe was transferred to a nitrocellulose filter paper to construct test paper, and the luminescent image was monitored by a homemade smartphone-based detection platform (Figure S9).[30,31] This novel nanoprobe-based test paper possesses two distinctive advantages. First, the test paper can emit two independent lights, which are red light and green light under 980 and 808 nm excitations, respectively. The emission intensities are able to be independently modulated by adjusting laser powers. Therefore, as shown in Figure 3a, the intensity ratios of green to red light can be flexibly tailored from 6:1 to 1:6 through modulation of the laser parameters (Table S1). Second, the patch difference is greatly reduced by use of the intensity ratios to depict the uniformity and stability of the test paper. For example, Figure 3b showed that the brightness of luminescent spots on different patches of test paper under 808 or 980 nm excitation seemed to be uniform. However, the detailed luminescent intensities of these spots actually demonstrated a significant difference with standard derivation ($\sigma$) values of 3.13 and 0.809 for green light and red light (Figure 3c,d), respectively. On the contrary, the intensity ratios of green to red emission of these 10 spots exhibited more uniform values, and the standard derivation value markedly decreased to 0.00122 (Figure 3e). On the basis of these advantages, it is more accurate to use intensity ratios to determine the target concentrations.

To demonstrate the superiority of this ratio-flexible modulated upconversion nanoprobe in the application of sensitive detection of exhaled NO, different intensity ratios of green to red emission were utilized to compare the luminescence changing behaviors after exposure of the test paper to same concentrations of NO gas. Intensity ratios were tailored from 1:1 to 1:3 and 1:6 by adjusting the 808 nm laser power while the 980 nm laser has a fixed power. In the case of 1:1, the green emission showed almost the same brightness with red emission, and different amounts of NO induced negligible intensity variations (Figure 4a). The corresponding intensity ratios also exhibited very small variations with the concentrations of NO changing from 5 to 25 ppb (Figure 4b). However, with decreasing the intensity ratios to 1:6, intensity ratios showed an obvious variation after exposure to the same amounts of NO. In addition, we have studied the influence of the adsorbance of Rd molecules in mesoporous silica toward luminescence quenching. It was found that quenching efficiencies obviously decreased after the adsorbance decreased to half or three-quarters of the saturated amounts (Figure S10). Therefore, saturated adsorption of Rd led to optimal detection sensitivity of 0.5 ppb in this work.

As a control, we have exploited a traditional yellow-emissive UCNP, $NaYF_4$:Yb/Er (48/2%), which gave out almost same intensities at green emission and red emission upon 980 nm excitation to construct a nanoprobe with Rd molecules. As shown in Figure S11, the luminescence quenching efficiency is much lower than the nanoprobe with the ratio of 1:6 at the same NO concentrations. The sensitivity of the traditional UCNPs-based probe is about 50 ppb, which is similar to the case of an intensity ratio of 1:1. Therefore, the sensitivity can be improved from 50 ppb at the condition of an intensity ratio of 1:1 or traditional UCNPs-based nanoprobes to 0.5 ppb when the intensity ratio changed to 1:6. The 100-fold sensitivity improvement should be ascribed to weaker green emission that was more sensitive toward trace amounts of analytes, while the red emission as the reference signal was still kept bright to guarantee the detection accuracy at the same time.

Ascribed to the flexible ratio-modulation, the nanoprobe also demonstrates a broad linear calibration range. In the case of an intensity ratio of 1:6, the weaker green emission was more sensitive toward lower concentrations of NO. As shown in Figure 4c and Figure S12, the intensity ratio variations exhibited a linear detection range from 0.5 to 25 ppb. After tailoring the intensity ratios to 1:3, green emission became brighter, and the linear quantitative detection range extended from 50 to 250 ppb (Figure 4d and Figure S13). Therefore, this ratio-modulated detection manner significantly broadened the probes' linear calibration ranges without changing the nanoprobe's constitution, making it become a robust tool for visualized sensitive detections of VOCs in exhaled breath, in which concentrations significantly vary from different individuals. To demonstrate the accuracy of this ratio-adjustable nanoprobe, the quantitative analysis according to the calibration curves through spiking with certain concentrations of NO gas are shown in Table S2. The detection experiment was repeated at least three times. It is found that the recoveries are satisfied for quantitative detection.

The application of this ratio-modulated nanoprobe for detection of nitric oxide in human exhalation was then evaluated through blind sample analysis. Eleven adult patients with serious clinical asthma symptoms from the First Affiliated Hospital of University of Science and Technology of China and 13 healthy volunteers participated in these evaluation experiments. The exhaled gas from these participants was collected in airbags with volume of 350 mL, into which the test paper was placed. Intensity ratio variations on the test paper after exposure to the exhaled gas were monitored by the smartphone-based detection device, and final concentrations were calculated according to the established correlation plots. The assayed concentrations of volatile NO for 24 specimens are shown in Figure 4e, which demonstrated that the probe could effectively identify the difference of NO concentrations in the exhaled breath from patients and healthy human according to the reported clinical cutoff threshold of 25 ppb.[4,32] Nevertheless, many reported works cannot detect the breath NO gas in health people, which is always in the subppb level.

## CONCLUSIONS

To sum up, a novel ratio-modulated fluorescent nanoprobe integrated with a smartphone analysis device was developed for rapid and sensitive detection of exhaled NO. Delightfully, in this novel ratiometric fluorescence nanoprobe, sensitivity can be improved by 100-fold through varying the intensity ratios while satisfying the high detection accuracy, and the linear responsive range is also greatly broadened. However, a few defects still remain to limit its practical applications. For


https://doi.org/10.1021/acs.analchem.1c01537
Anal. Chem. XXXX, XXX, XXX−XXX

example, a user-friendly smartphone app needs to be exploited for rapid and accurate analysis of luminescent signal variations on the test paper for in-field applications. In addition, a few standard devices, such as the breath-collected airbag, should be developed to make the detection more operational for practical applications. It is anticipated that this work will inspire new designs of ratiometric fluorescence probes and facilitate the advancement of cost-effective paper-based devices for point-of-care detection of a spectrum of biomarkers for disease diagnosis.

## ■ ASSOCIATED CONTENT

### Supporting Information

The Supporting Information is available free of charge at https://pubs.acs.org/doi/10.1021/acs.analchem.1c01537.

Synthesis procedures of nanocrystals and NO recognition molecules, preparation of test paper, mass spectra, TEM images of the UCNPs, luminescence variations of the nanoprobes upon additions of different interference anion ions, and luminescent images of the test paper after exposure to different amounts of NO (PDF)

## ■ AUTHOR INFORMATION


### Corresponding Author

**Qingsong Mei** − *School of Medicine, Jinan University, Guangzhou, Guangdong 510632, China;* orcid.org/0000-0003-4327-6931; Email: qsmei@jnu.edu.cn

### Authors

**Jianxiong Zhou** − *School of Food and Biological Engineering, Hefei University of Technology, Hefei, Anhui 230009, China*

**Ruiying Wu** − *Department of Traditional Chinese Medicine, The First Affiliated Hospital of University of Science and Technology of China, Hefei, Anhui 230001, China*

**Xiao Fu** − *School of Food and Biological Engineering, Hefei University of Technology, Hefei, Anhui 230009, China*

**Jinmei Wu** − *School of Food and Biological Engineering, Hefei University of Technology, Hefei, Anhui 230009, China*

Complete contact information is available at: https://pubs.acs.org/10.1021/acs.analchem.1c01537

### Author Contributions

‖J.Z. and R.W. contributed equally.


### Notes

The authors declare no competing financial interest.

## ■ ACKNOWLEDGMENTS

The work was supported by the grants from the National Natural Science Foundation of China (Grants 21675038 and 22074028).

## ■ REFERENCES


(1) Bruderer, T.; Gaisl, T.; Gaugg, M. T.; Nowak, N.; Streckenbach, B.; Muller, S.; Moeller, A.; Kohler, M.; Zenobi, R. *Chem. Rev.* **2019**, *119* (19), 10803−10828.

(2) Kim, S.-J.; Choi, S.-J.; Jang, J.-S.; Cho, H.-J.; Kim, I.-D. *Acc. Chem. Res.* **2017**, *50* (7), 1587−1596.

(3) Hu, Z. G.; Zhang, H. Y.; Hu, K.; Song, X. Y. *J. Breath. Res.* **2021**, *15* (2), 026008.

(4) Ulrik, C. S.; Lange, P.; Hilberg, O. *Eur. Clin. Respir. J.* **2021**, *8* (1), 1891725.

(5) Lane, C.; Knight, D.; Burgess, S.; Franklin, P.; Horak, F.; Legg, J.; Moeller, A.; Stick, S. *Thorax* **2004**, *59* (9), 757−760.

(6) Nerpin, E.; Olivieri, M.; Gislason, T.; Olin, A. C.; Nielsen, R.; Johannessen, A.; Ferreira, D. S.; Marcon, A.; Cazzoletti, L.; Accordini, S.; Pin, I.; Corsico, A.; Demoly, P.; Weyler, J.; Nowak, D.; Jogi, R.; Forsberg, B.; Zock, J. P.; Sigsgaard, T.; Heinric, J.; Bono, R.; Leynaert, B.; Jarvis, D.; Janson, C.; Malinovschi, A. *Clin. Exp. Allergy* **2019**, *49* (7), 969−979.

(7) Tsikas, D. *Anal. Chem.* **2000**, *72* (17), 4064−4072.

(8) Yao, H. W.; Guo, X. F.; Wang, H. *Anal. Chem.* **2020**, *92* (17), 11904−11911.

(9) Tu, F. Q.; Zhang, L. Y.; Guo, X. F.; Zhang, Z. X.; Wang, H.; Zhang, H. S. *J. Chromatogr. A* **2014**, *1359*, 309−316.

(10) Wang, N.; Yu, X.; Zhang, K.; Mirkin, C. A.; Li, J. *J. Am. Chem. Soc.* **2017**, *139* (36), 12354−12357.

(11) Zhao, C. Y.; Chen, J. X.; Zhong, R. B.; Chen, D. S.; Shi, J. J.; Song, J. B. *Angew. Chem., Int. Ed.* **2021**, *60* (18), 9804−9827.

(12) Zhang, Z. M.; Shikha, S.; Liu, J. L.; Zhang, J.; Mei, Q. S.; Zhang, Y. *Anal. Chem.* **2019**, *91* (1), 548−568.

(13) Lucky, S. S.; Soo, K. C.; Zhang, Y. *Chem. Rev.* **2015**, *115* (4), 1990−2042.

(14) Zhou, L.; Wang, R.; Yao, C.; Li, X.; Wang, C.; Zhang, X.; Xu, C.; Zeng, A.; Zhao, D.; Zhang, F. *Nat. Commun.* **2015**, *6*, 6938.

(15) Mei, Q.; Zhang, Z. *Angew. Chem., Int. Ed.* **2012**, *51* (23), 5602−5606.

(16) Ma, T.; Hou, Y.; Zeng, J.; Liu, C.; Zhang, P.; Jing, L.; Shangguan, D.; Gao, M. *J. Am. Chem. Soc.* **2018**, *140* (1), 211−218.

(17) Wang, J.; Li, D. Q.; Ye, Y. X.; Qiu, Y.; Liu, J. W.; Huang, L.; Liang, B.; Chen, B. L. *Adv. Mater.* **2021**, *33* (15), 2008020.

(18) Luo, Z. J.; Lv, T. Y. Z.; Zhu, K. N.; Li, Y.; Wang, L.; Gooding, J. J.; Liu, G. Z.; Liu, B. *Angew. Chem., Int. Ed.* **2020**, *59* (8), 3131−3136.

(19) Wu, S. Y.; Min, H.; Shi, W.; Cheng, P. *Adv. Mater.* **2020**, *32* (3), 1805871.

(20) Sedgwick, A. C.; Wu, L. L.; Han, H. H.; Bull, S. D.; He, X. P.; James, T. D.; Sessler, J. L.; Tang, B. Z.; Tian, H.; Yoon, J. *Chem. Soc. Rev.* **2018**, *47* (23), 8842−8880.

(21) Liu, L.; Wang, S. F.; Zhao, B. Z.; Pei, P.; Fan, Y.; Li, X. M.; Zhang, F. *Angew. Chem., Int. Ed.* **2018**, *57* (25), 7518−7522.

(22) Yin, H. Q.; Yin, X. B. *Acc. Chem. Res.* **2020**, *53* (2), 485−495.

(23) Sun, Z. B.; Liu, J. K.; Yuan, D. F.; Zhao, Z. H.; Zhu, X. Z.; Liu, D. H.; Peng, Q.; Zhao, C. *Angew. Chem., Int. Ed.* **2019**, *58* (15), 4840−4846.

(24) Dong, H.; Du, S. R.; Zheng, X. Y.; Lyu, G. M.; Sun, L. D.; Li, L. D.; Zhang, P. Z.; Zhang, C.; Yan, C. H. *Chem. Rev.* **2015**, *115* (19), 10725−815.

(25) He, S.; Johnson, N. J. J.; Nguyen Huu, V. A.; Cory, E.; Huang, Y.; Sah, R. L.; Jokerst, J. V.; Almutairi, A. *Nano Lett.* **2017**, *17* (8), 4873−4880.

(26) Wisser, M. D.; Fischer, S.; Siefe, C.; Alivisatos, A. P.; Salleo, A.; Dionne, J. A. *Nano Lett.* **2018**, *18* (4), 2689−2695.

(27) Guo, X. R.; Yuan, Y.; Liu, J. L.; Fu, S.; Zhang, J.; Mei, Q. S.; Zhang, Y. *Anal. Chem.* **2021**, *93* (5), 3010−3017.

(28) Mei, Q. S.; Bansal, A.; Jayakumar, M. K. G.; Zhang, Z. M.; Zhang, J.; Huang, H.; Yu, D. J.; Ramachandra, C. J. A.; Hausenloy, D. J.; Soong, T. W.; Zhang, Y. *Nat. Commun.* **2019**, *10*, 4416.

(29) Lei, Z. D.; Ling, X.; Mei, Q. S.; Fu, S.; Zhang, J.; Zhang, Y. *Adv. Mater.* **2020**, *32* (9), 1906225.

(30) Mei, Q.; Jing, H.; Li, Y.; Yisibashaer, W.; Chen, J.; Nan Li, B.; Zhang, Y. *Biosens. Bioelectron.* **2016**, *75*, 427−432.

(31) Chen, X.; Mei, Q. S.; Yu, L.; Ge, H.; Yue, J.; Zhang, K.; Hayat, T.; Alsaedi, A.; Wang, S. *ACS Appl. Mater. Interfaces* **2018**, *10* (49), 42225−42232.

(32) Dweik, R. A.; Boggs, P. B.; Erzurum, S. C.; Irvin, C. G.; Leigh, M. W.; Lundberg, J. O.; Olin, A.-C.; Plummer, A. L.; Taylor, D. R. *Am. J. Respir. Crit. Care Med.* **2011**, *184* (5), 602−615.

**Supporting Information**

# Ratio-Adjustable Upconversion Luminescence Nanoprobe for Ultrasensitive in-Vitro Diagnostics

Jianxiong Zhou,[‡] Ruiying Wu,[‡] Xiao Fu, Jinmei Wu, and Qingsong Mei*

J. Zhou, X. Fu, J. Wu

School of Food and Biological Engineering

Hefei University of Technology

Hefei, Anhui 230009, China

Prof. Q. Mei

School of Medicine

Jinan University

Guangzhou, Guangdong 510632, China

E-mail: qsmei@jnu.edu.cn

Dr. R. Wu

Department of Traditional Chinese Medicine

The First Affiliated Hospital of University of Science and Technology of China

Hefei, Anhui 230001, China

[‡] These authors contributed equally to this work.

# Table of contents

**Figure S1.** TEM images of the nanoparticles. S6

**Figure S2.** XRD, FTIR and Zeta potential of the nanoprobe. S7

**Figure S3.** Absorption spectra and corresponding linear plot of Rd molecules. S7

**Figure S4.** The absorption spectra of the nanoprobe before and after exposure to NO. S8

**Scheme S1.** Synthesis route of Rd molecules. S8

**Figure S5.** Mass spectrum of Rd molecules. S9

**Figure S6.** Reaction mechanism between Rd and NO molecules, and mass spectrum of the reaction product. S9

**Figure S7.** Luminescence quenching efficiency at green or red emissions. S10

**Figure S8.** Selectivity investigation of the nanoprobes. S11

**Figure S9.** Front view and back view of the smartphone-based detection setup. S12

**Table S1.** The detailed parameters of the excitation lasers. S12

**Figure S10.** Detection of exhaled NO gas by use of the nanoprobe constructed with different amounts of adsorbed Rd molecules. S13

**Figure S11.** Luminescence quenching efficiency of traditional yellow emissive UCNPs. S13

**Figure S12.** The luminescent images of the data in Figure 4c. S14

**Figure S13.** The luminescent images of the data in Figure 4d. S14

**Table S2.** Recovery test of NO gas by the ratio-adjustable nanoprobe. S14

**Figure S14.** Luminescence quenching efficiency of the test paper after exposure to the species that may exist in exhalation. S15

# Experimental Section

## 1. Materials and Instruments.

Rare-earth oxides, $Y_2O_3$, $Yb_2O_3$, $Er_2O_3$, $Tm_2O_3$, $Nd_2O_3$, tetraethyl orthosilicate (TEOS), aminopropyl trimethoxysilane (APTS), l-phenylenediamine and Rhodamine B were purchased from Aladdin (Shanghai, China). The rare earth oxides were reacted with excess acetic acid at 100 °C for 24 hours to obtain their acetates. NaF, $Na_2CO_3$, $NaNO_2$, NaClO, $H_2O_2$, $NH_4NO_3$, cetyltrimethyl ammonium bromide (CTAB), 1-propylphosphate cyclic anhydride DMF solution, acetic acid, dichloromethane, ethanol and other commonly used solvents were obtained from Sinopharm Chemical Reagent Co., Ltd. (Shanghai, China).

Commercial NO gas was purchased from Nanjing Special Gas Factory Co., Ltd., China. For the aqueous solution-based detection, NO gas was bubbled into deoxidized PBS solution to obtain NO-saturated PBS solution. It has been well studied that the ice-cooled saturated concentration of NO is about 2 mM.[1] For NO gas detection, different amounts of the commercial NO gas were bubbled into a nitrogen-protected sealed glass bottle through a flowmeter. Hydroxy radical was produced through the classical Fenton reaction, by adding ferrous sulfate in the presence of 10 equivalent of hydrogen peroxide in de-aerated solution before use. Its concentration was quantified through the concentration of ferrous sulfate. All of stock solution or gas samples were freshly prepared for each experiment.

Luminescence spectra were recorded on a Peking-Elmer LS-55 spectrometer equipped with 980 nm and 808 nm lasers. UV-vis absorption spectra were examined on UV 9000s spectrophotometer.

## 2. Synthesis of NO recognition molecules, Rd.

1 g of rhodamine B and 0.86 g of l-phenylenediamine were dissolved in 30 mL of dichloromethane. 1.5 mL of triethylamine and 3 mL of 1-propylphosphate cyclic anhydride DMF solution (50 wt. %) were added into the above mixture, and subsequently reacted at 50 °C for 12 hours. The crude product was purified by silica gel chromatography ($CH_2Cl_2$:MeOH=30:1, v/v) to obtain the NO recognition molecules Rd.

3. **Synthesis of mesoporous silica coated nanoparticles (mUCNPs).**

The orthogonal emissive UCNPs, $NaErF_4$:Yb (19.5%), Tm (0.5%) @ $NaYF_4$:Yb (10%) @ $NaNdF_4$:Yb (10%), were synthesized by thermal decomposition and layer by layer injection protocols as we reported before.[2] Mesoporous silica shell was coated onto the surface of UCNPs through sol-gel strategy. Typically, 200 mg of CTAB was dissolved in 20 mL of water. 0.15 mmol of UCNPs in cyclohexane was added into above solution, and kept stirring overnight. After the solution became transparent, 40 mL of water and 6 mL of ethanol were added into above solution. Then, 0.3 mL of concentrated ammonia were added, and the mixture was stirred for 30 minutes. 0.3 mL of TEOS were subsequently dropped into the mixture and refluxed for 1 h. The nanoparticles were obtained by centrifugation, washing with ethanol for three times, and re-dispersing in ethanol. To form mesoporous silica, the resulted nanoparticles were mixed within 600 mg ammonium nitrate in 30 mL of ethanol solution, and refluxed at 60 °C for 6 hours. Finally, mUCNPs were acquired by centrifugation and washing.

To synthesis of NO-responsive nanoprobes, 40 mg of Rd was dissolved in 20 mL of ethanol by ultrasonication, then the dried mUCNPs were added into the solution, and stirred at room temperature overnight. The nanoprobes were then obtained through centrifugation and washing to remove the adsorbing Rd.

4. **Preparation of test paper and monitoring the luminescence signals by a smartphone-based detection platform.**

The nitrocellulose filter paper was cut into rectangular shape with a size of 3 cm × 1 cm. The filter paper was then immersed into nanoprobe PBS solution with ultrasonication for few minutes, and then taken out for drying in an oven overnight to prepare the test paper.

The smartphone-based detection platform was fabricated as we reported before.[3] Specifically, a smartphone, lasers with the emitted wavelength at 980 nm or 808 nm, optical filter for filtrating excitation wavelength, and test paper were orderly assembled in an accessory. The luminescence signals on test paper were monitored by the smartphone camera, and the emission intensity variations of test paper after exposure to different amounts of NO were analyzed by Image J software.

5. **Detection of exhaled NO gas.**

11 adult patients with serious clinical asthma symptoms from the First Affiliated Hospital of University of Science and Technology of China and 13 healthy volunteers participated this evaluation experiments. The test paper prepared in the same batch were first numbered and placed in airbags with volume of 350 mL. During the testing period, volunteers were asked to blow the compressed airbags to the maximum volume. The airbags were then tightened to let exhaled gas contact with the test paper for about 10 minutes. At last, test paper was collected and dried properly. The luminescence variations on the test paper were recorded and analyzed by the smartphone-based detection system.

## Supporting Figures

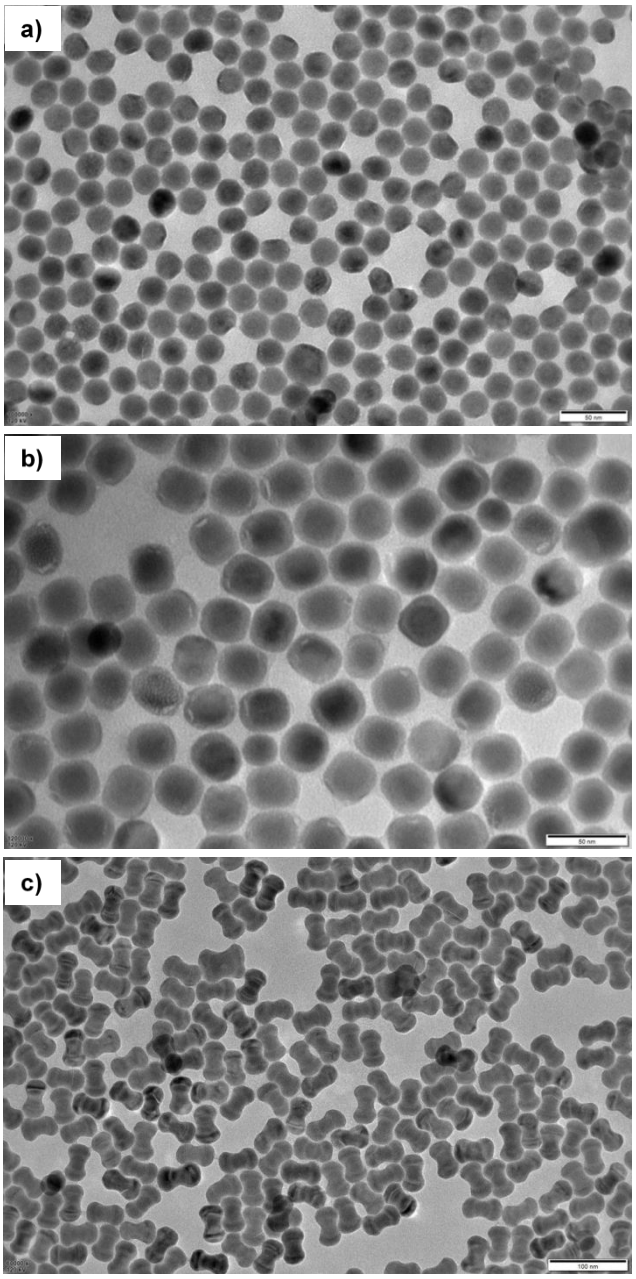


**Figure S1.** TEM images of (a) core nanoparticles $NaErF_4$: Yb/Tm, (b) core-shell nanoparticles $NaErF_4$: Yb/Tm@$NaYF_4$: Yb, and (c) the final core-shell-shell nanoparticles $NaErF_4$: Yb/Tm@$NaYF_4$: Yb@$NaNdF_4$: Yb.

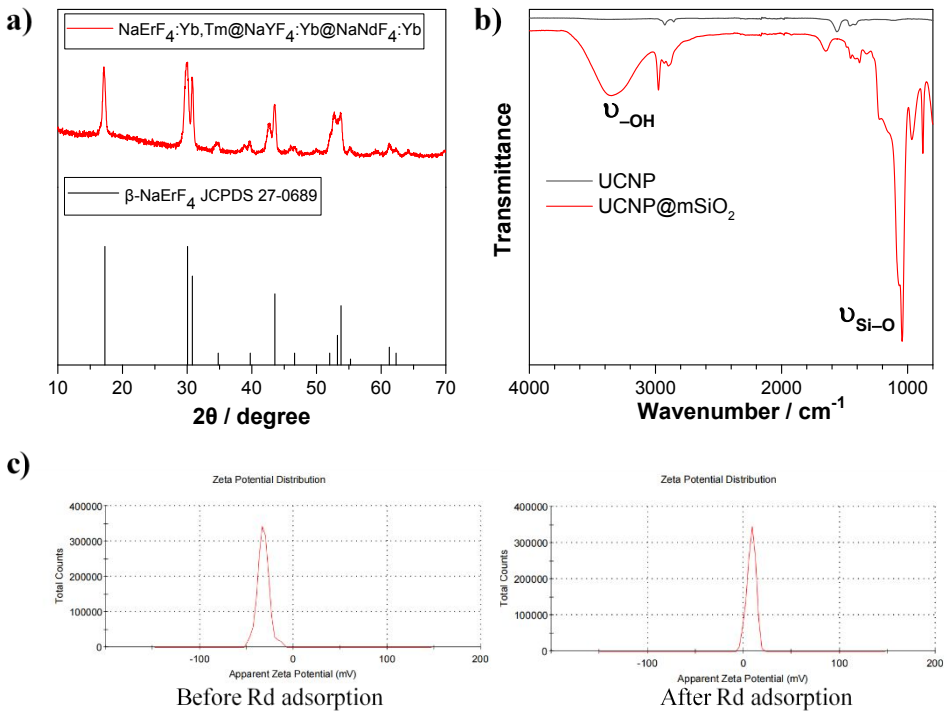


**Figure S2.** (a) XRD pattern of the obtained core-shell-shell structured UCNPs. (b) FTIR spectra of the UCNPs before and after coating of mesoporous silica. (c) Zeta potential of mUCNPs before and after adsorption of Rd molecules.

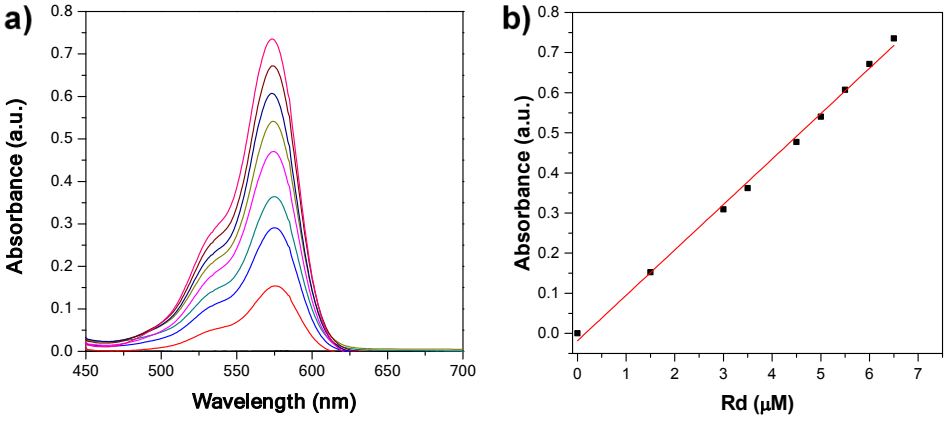


**Figure S3.** (a) The absorption spectra variations of different amounts of Rd molecules after addition of excess NO. The concentrations of Rd from bottom to top are 0, 1.5, 3, 3.5, 4.5, 5, 5.5, 6, 6.5 μM. (b) The corresponding linear plot of absorption versus Rd concentrations.

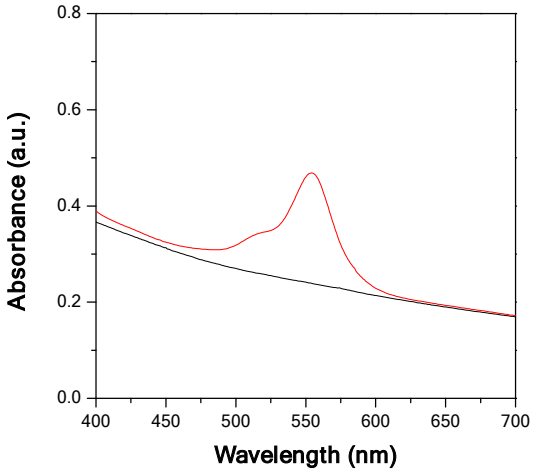


**Figure S4.** The absorption spectra of mUCNPs in PBS solution (black line) and the Rd-modified mUCNPs after exposure to excess NO (red line) at same concentrations. The saturated absorbed amount of Rd molecules was calculated to be 4.4 mmol Rd per 1 mmol mUCNPs according to the linear plot in Figure S3b.

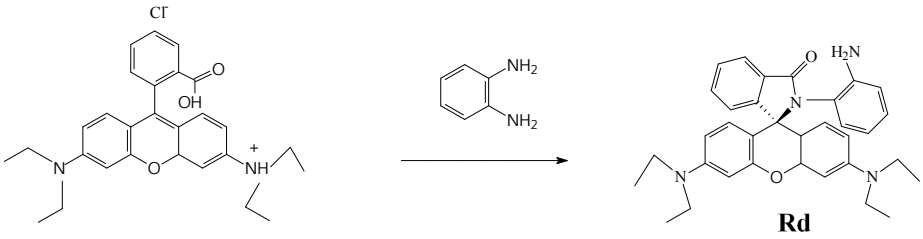


**Scheme S1.** Schematic illustrations for the synthesis route of Rd molecules.

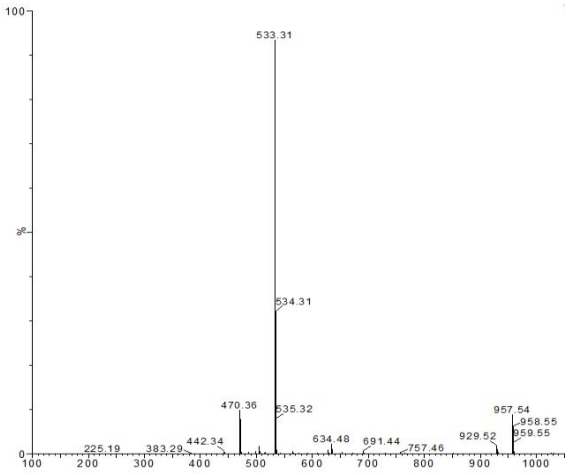


**Figure S5.** Mass spectrum of Rd molecules.

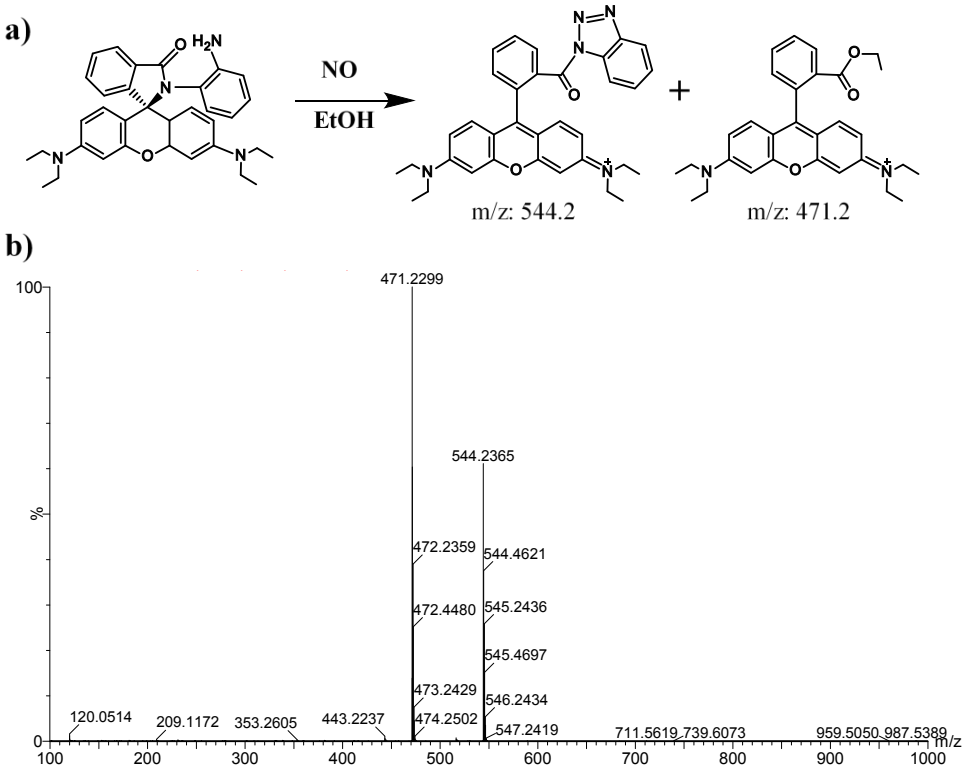


**Figure S6.** (a) Schematic illustrations for the reaction between Rd and NO molecules. (b) Mass spectrum of the reaction product.

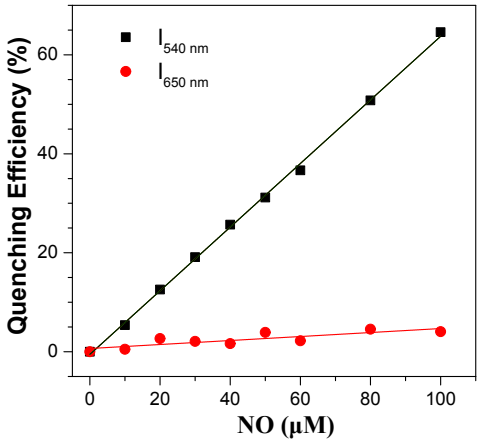


**Figure S7.** The comparison of luminescence quenching efficiency at green or red emissions of the nanoprobe in aqueous solution towards different amounts of NO.

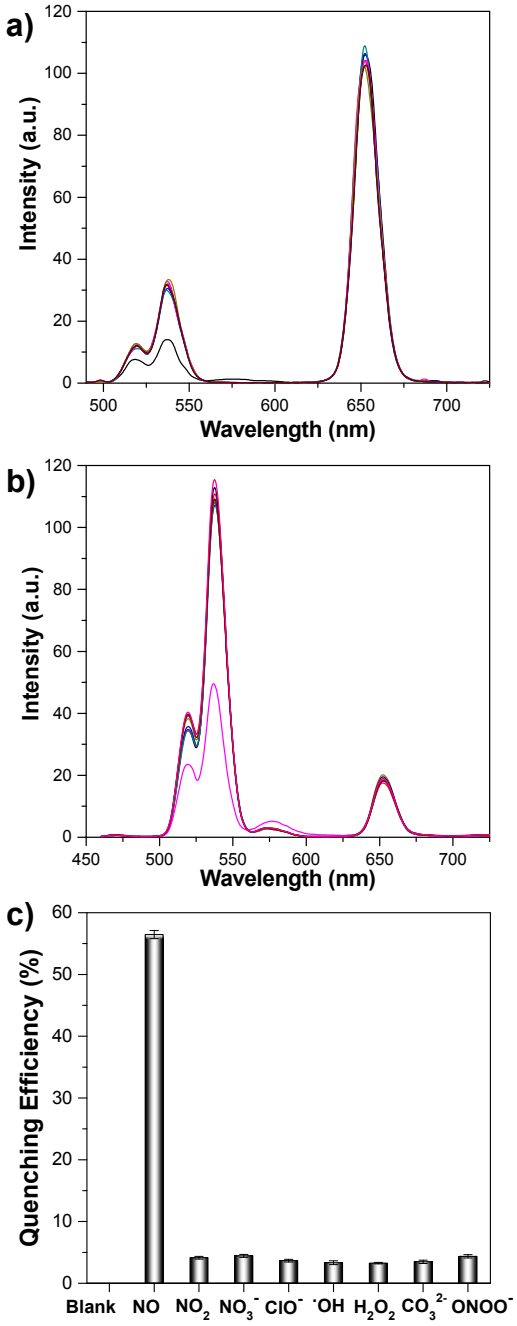


**Figure S8.** Selectivity investigation of the nanoprobes. Luminescence variations of the nanoprobe after additions of various interference ions with concentrations of 0.1 mM, including ·OH, $ClO^-$, $CO_3^{2-}$, $H_2O_2$, NO, $NO_2^-$, $NO_3^-$ and $ONOO^-$ upon excitation at 980 nm (a) and 808 nm (b). (c) Luminescence quenching efficiency of the nanoprobe towards various anion ions.

**Figure S9.** Front view and back view of the smartphone-based detection setup.

**Table S1.** The detailed parameters of the excitation lasers for modulation of emission ratios.

| Intensity ratio of green to red emission | Power of 980 nm laser (W) | Power of 808 nm laser (W) |
|---|---|---|
| 6:1 | 1 | 2.5 |
| 3:1 | 1.25 | 2.5 |
| 1:1 | 1.5 | 2.5 |
| 1:3 | 1.5 | 2 |
| 1:6 | 1.5 | 1.5 |

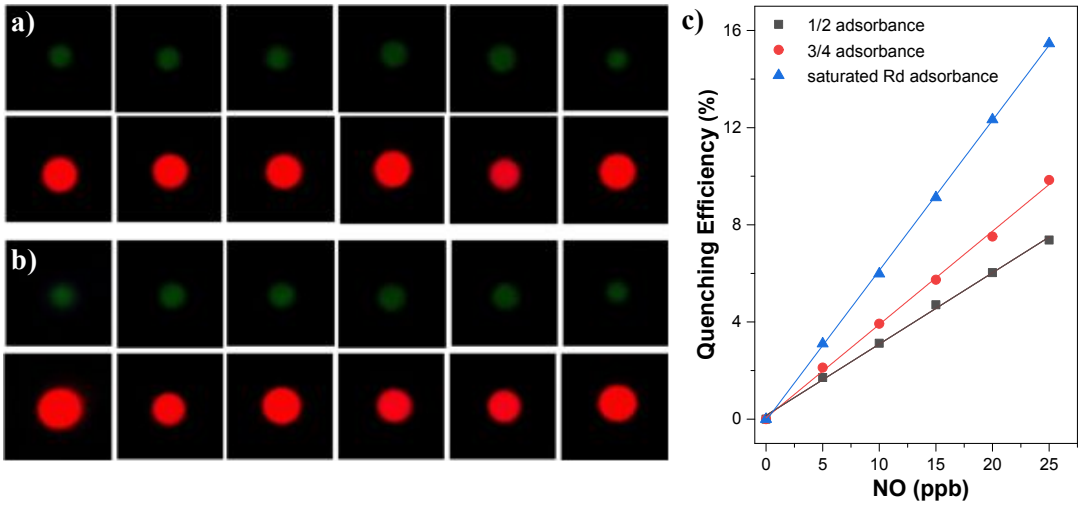


**Figure S10.** Detection of exhaled NO gas by use of the nanoprobe constructed with different amounts of adsorbed Rd molecules, a) three quarters saturated adsorbance and b) half saturated adsorbance. The amounts of NO from left to right are 0, 5, 10, 15, 20 and 25 ppb for each panel, respectively. (c) The corresponding quenching efficiency of test paper at different Rd adsorbance in mUCNPs at the intensity ratio of 1:6.

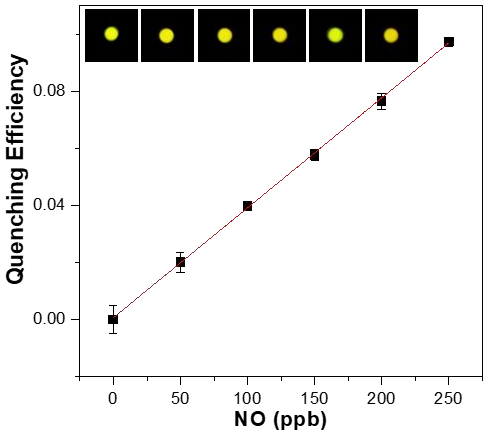


**Figure S11.** Luminescence quenching efficiency of traditional yellow emissive UCNPs, $NaYF_4$:Yb/Er (48/2%) based test paper towards different concentrations of NO.

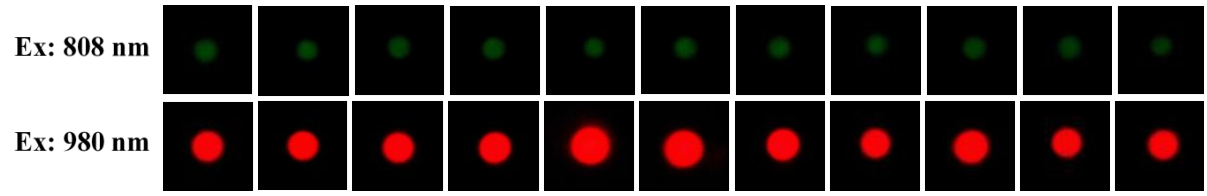


**Figure S12.** The luminescent images of the data in Figure 4c. Intensity ratio of green to red emission is 1:6. The NO concentrations exposed to test paper are 0, 0.5, 1, 1.5, 2, 2.5, 5, 10, 15, 20, 25 ppb from left to right.

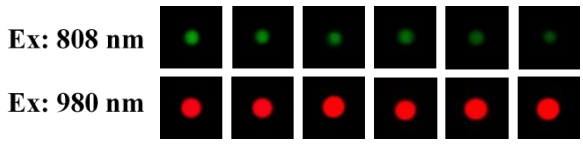


**Figure S13.** The luminescent images of the data in Figure 4d. Intensity ratio of green to red emission is 1:3. The NO concentrations exposed to test paper are 0, 50, 100, 150, 200, 250 ppb from left to right.

**Table S2.** Recovery test of NO gas by the ratio-adjustable nanoprobe.

| Spiked ( ppb ) | Calculated ( ppb ) | Recovery ( % ) | RSD ( %, n=3 ) |
|---|---|---|---|
| 10 | 10.23 | 102.3 | 2.415 |
| 20 | 20.26 | 101.3 | 1.589 |
| 50 | 49.65 | 99.30 | 0.8672 |
| 100 | 100.1 | 100.1 | 0.4889 |

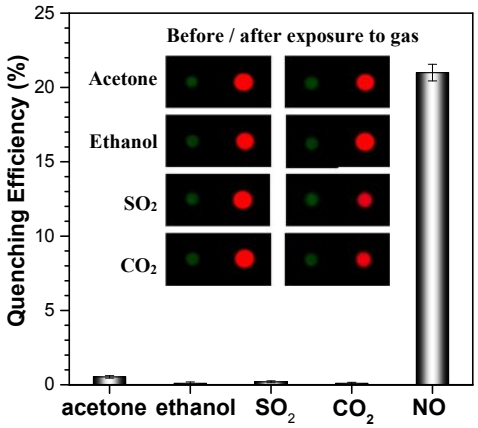


**Figure S14.** Luminescence quenching efficiency of the test paper after exposure to the species that may exist in exhalation. The concentration for every species was 200 ppb. Inset images are the luminescent photos of test paper before and after exposure to different gas under 808 nm and 980 nm excitation. The quenching efficiency of NO was derived from the data in Figure 4d.

# References


[1] Vegesna, G. K.; Sripathi, S. R.; Zhang, J. T.; Zhu, S. L.; He, W. L.; Luo, F. T.; Jahng, W. J.; Frost, M.; Liu, H. Y., Highly Water-Soluble BODIPY-Based Fluorescent Probe for Sensitive and Selective Detection of Nitric Oxide in Living Cells. *Acs Applied Materials & Interfaces* **2013,** *5* (10), 4107-4112.

[2] Q. S. Mei, A. Bansal, M. K. G. Jayakumar, Z. M. Zhang, J. Zhang, H. Huang, D. J. Yu, C. J. A. Ramachandra, D. J. Hausenloy, T. W. Soong, Y. Zhang, Manipulating energy migration within single lanthanide activator for switchable upconversion emissions towards bidirectional photoactivation. *Nature Communications* **2019**, *10*, 4416.

[3] Q. S. Mei, H. Jing, Y. Li, W. Yisibashaer, J. Chen, B. N. Li, Y. Zhang, Smartphone based visual and quantitative assays on upconversional paper sensor. *Biosens. Bioelectron.* **2016**, *75*, 427-432.